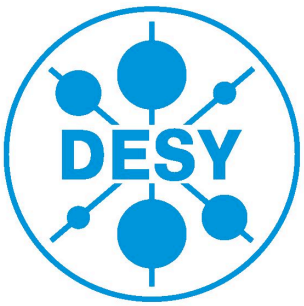

Calibration of Alibava Readout System for Lorentz Angle Measurement Experiment

Ahmed Abouelfadl, Assiut University, Egypt

September 4, 2013

Supervisior: Eda Yildirim, DESY ATLAS group

Abstract

The High Luminosity-LHC is a major upgrade to the Large Hadron Collider (LHC) in CERN. With this upgrade the luminosity (rate of collisions) will be increased by a factor of ten around the year of 2020. The high luminosity at HL-LHC will lead to increase in radiation damage in the ATLAS inner detector (ID). The Lorentz angle measurement experiment investigates the effects of high radiation on the Lorentz angle, which is important to reconstruct particle tracks and momentum accurately. In the Lorentz angle measurement experiment the Alibava readout system is used to readout of sensors. Due to setup complexity, some setup parameters may change the signal amplitude per channel. In this report, I present calibration corrections of Alibava signal.

Contents

1 Introduction **3**
1.1 The ATLAS experiement 3
1.2 The ATLAS Inner Detector (ID) 4
1.3 The High Luminosity LHC 4

2 The Lorentz Angle Measurement experiment **6**
2.1 Experiment Setup 9
2.2 The Alibava Readout System 9
2.3 Motivation 11

3 Calibration of Alibava Readout System **12**
3.1 Method and Procedure 12
3.2 Monitoring of DUT parameters 13
3.3 Software updates 13

4 Results **16**

5 Conclusion **21**

6 Acknowledgments **21**

7 Appendix: Monitoring of DUT parameters using NI LabView **22**

1 Introduction

1.1 The ATLAS experiement

ATLAS (A Toroidal LHC Apparatus) is one of two general purpose detectors at the Large Hadron Collider in CERN, shown in [Figure 1]. The Atlas detector consists of four major parts :

The magnet configuration is based on an inner superconducting solenoid around the inner detector cavity, and large superconducting air-core toroids consisting of independent coils arranged with an eight-fold symmetry outside the calorimetry.

The inner detector is contained within a cylinder of length 6.80 m and radius 1.15 m, with a solenoidal magnetic field of 2 T. Pattern recognition, 10^2 momentum and vertex measurements, and enhanced electron identification are achieved with a combination of discrete high-resolution pixel and strip detectors in the inner part and continuous straw-tube tracking detectors with transition radiation capability in the outer part of the tracking volume.

The calorimeters are situated outside the solenoidal magnet that surrounds the Inner Detector. Their purpose is to measure the energy from particles by absorbing it. There are two basic calorimeter systems: an inner electromagnetic calorimeter and an outer hadronic calorimeter. Both are sampling calorimeters; that is, they absorb energy in high-density metal and periodically sample the shape of the resulting particle shower, inferring the energy of the original particle from this measurement.

The muon spectrometer defines the overall dimensions of the ATLAS detector. The outer chambers of the barrel are at a radius of about 11 m. The length of the barrel toroid coils is 13 m, and the third layer of the forward muon chambers, mounted on the cavern wall, is located at 21 m from the interaction point. The overall weight of the ATLAS detector is about 7000 tons [1].

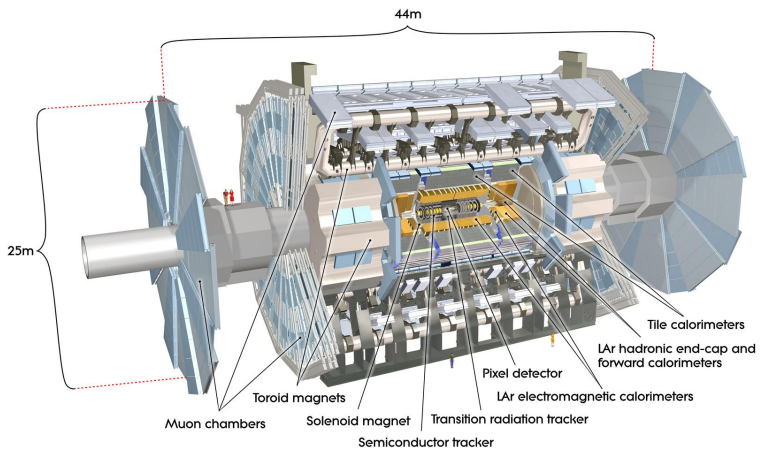

Figure 1: A computer generated picture of the ATLAS Detector [1]

1.2 The ATLAS Inner Detector (ID)

The current ATLAS Inner Detector tracker [Figure 2] is made out of three detector types, moving inside out we find:
(a) The silicon Pixel detector
(b) The SemiConductor Tracker (SCT)
(c) The Transition Radiation Tracker (TRT)
All these detectors allow precision measurement of charged particle trajectories in the environment of numerous tracks, but the Pixel mainly contributes to measure vertices accurately, the SCT to measure precisely the particle momenta and the TRT to ease the pattern recognition with its very large number of close hits (while also contributing to electron identification). The figure illustrates the layout and shows that each detector consists of barrel and end cap regions in order to minimize the material traversed by particles coming from the interaction vertex [2].

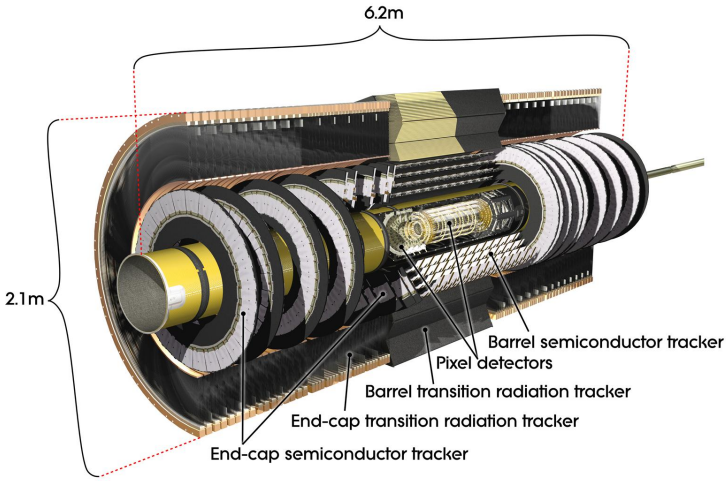

Figure 2: The ATLAS Inner Detector

1.3 The High Luminosity LHC

In the next few years, the LHC will undergo a series of upgrades towards the High-Luminosity LHC (HL-LHC) [Figure 3], leading ultimately by the year of 2024 to an instantaneous luminosity of $5 \times 10^{34} cm^2 s^{-1}$. At the end of HL-LHC run time, the expected total integrated luminosity is about 3000 fb^{-1}.
The increased instantaneous luminosity at the HL-LHC results in the expected mean number of interactions per bunch crossing increasing from ~ 55 at $2 \times 10^{34} cm^2 s^{-1}$ to ~ 140 at $5 \times 10^{34} cm^2 s^{-1}$ (assuming a bunch crossing time of 25 ns) and the consequent increase in the integrated luminosity requires a detector able to operate after exposure to large particle fluences. To allow for some safety margin, the design studies for the

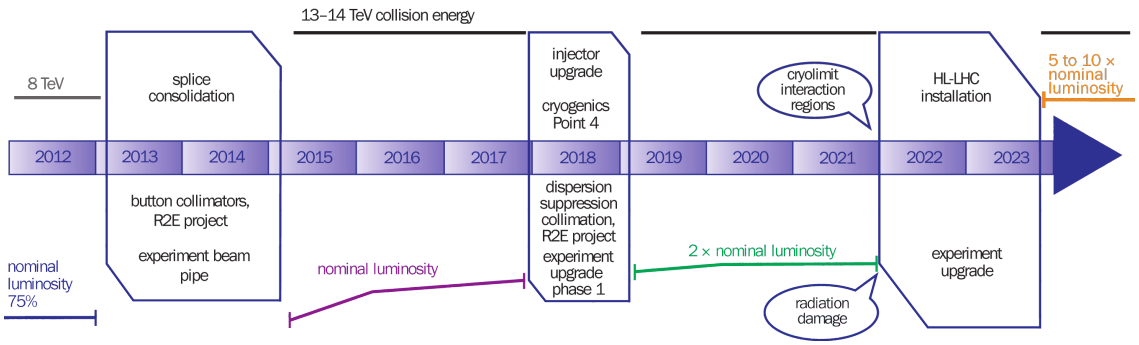

Figure 3: Timeline of the upgrades leading to the High Luminosity LHC

proposed upgrades assume a maximum instantaneous luminosity of $7 \times 10^{34} cm^2 s^{-1}$. This will require upgrades for ATLAS detector, for example the inner detector will be replaced with silicon only system. The current pixel detector was designed using radiation hard sensors and electronics technologies to withstand 10^{15} n_{eq}/cm^2 (1 MeV neutron equivalent per square centimeter). This is estimated to correspond to 400 fb^{-1}. The SCT detector for example can operate up to a fluence of $2 \times 10^{14} n_{eq}/cm^2$, which is significantly lower than the $\sim 10^{15} n_{eq}/cm^2$ required at the HL- LHC. The expected Radiation levels at the new HL-LHC inner detector has been calculated with radiation background simulations [Figure 4] [7].

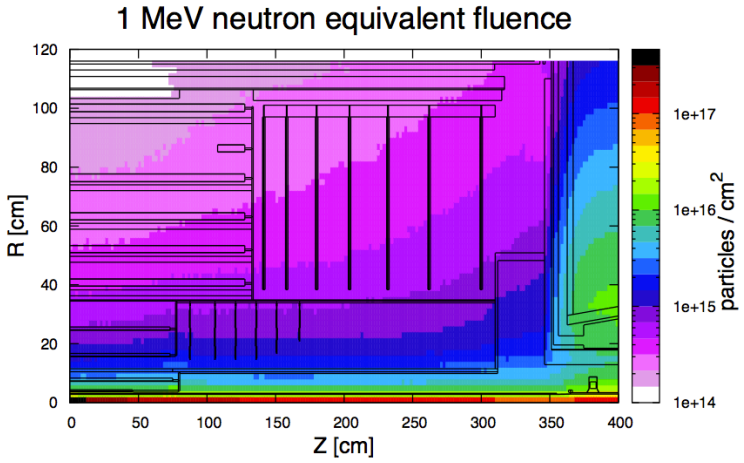

Figure 4: Background Radiation simulations

The HL-LHC operation will allow for studies of the properties of the new Higgs-like boson at the LHC [Figure 5]: Yukawa and self-couplings, spin and CP quantum numbers etc. It will extend the energy scales that can be studied in high energy boson-boson scattering, to study electroweak symmetry breaking mechanism and to probe for signatures of new physics predicted by models such as SUSY and extra dimensions into the multi-TeV. [3]

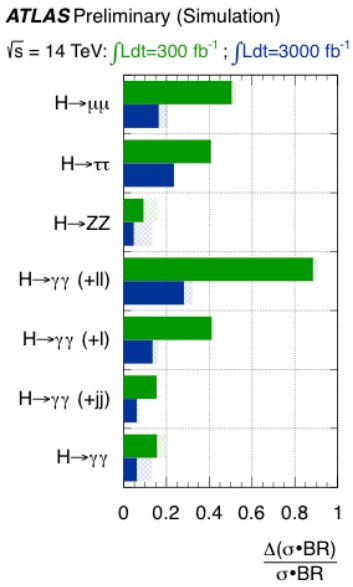

Figure 5: Expected measurement precision on the signal strength in all considered channels for luminosities of 300 fb^{-1} and 3000 fb^{-1} [4]

2 The Lorentz Angle Measurement experiment

The passage of energetic charged particles in semi-conductor detectors will produce pairs of electrons and holes. In the absence of magnetic field, the direction of the charge carrier is determined by the electric field created from the bias voltage applied at the detector. These charge carriers drift to the electrodes. The drift (current) creates the signal which is amplified by an amplifier connected to each strip. Particles passing with inclined angles will create a signal at a number of channels corresponding to cluster size which is $\tan(\theta_i) \times t$. where θ_i is the incident angle and t is the thickness of the detector [5]. [Figure 6]

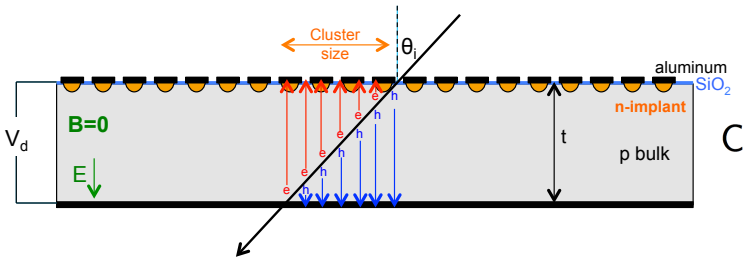

Figure 6: Charged particle going through silicon sensor with incident angle θ_i under 0 Magnetic field

For detectors under magnetic field, the field will deflect the charge carriers increasing

the cluster size.[Figure 7]

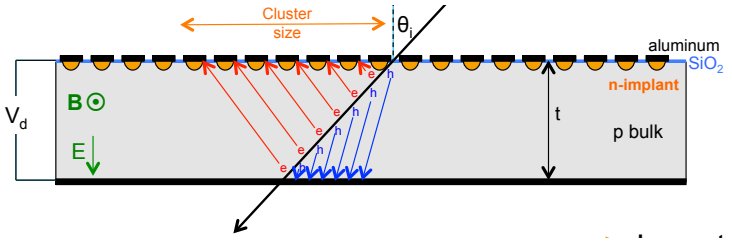

Figure 7: Charged particle going through silicon detector with incident angle θ_i under Magnetic field

The Angle by which charge carriers in a silicon sensor are deflected under magnetic field is called the Lorentz angle θ_L .
The Lorentz angle needs to be taken into account for the accurate reconstruction of particle tracks and momentum. The knowledge of this angle is thus needed for a correct simulation of the detector response and for an understanding of alignment systematics at the level required for a precision measurement of W mass for example.
The Lorentz Angle can be calculated from

$$\tan(\theta_L) = \mu_H \cdot B = r_h \cdot \mu_d \cdot B \tag{1}$$

where (μ_H) is the Hall mobility and (μ_d) is the drift mobility. Their ratio r_h is called Hall factor and depends on the details of the scattering mechanism of charge carriers in silicon. It is a pure number of order unity [6].
The drift mobility(μ_d) can be caluclated from

$$\mu_d = \frac{v_s/E_c}{[1 + [E/E_c]^{\beta}]^{1/\beta}} \tag{2}$$

where v_s is the drift velocity, E is electric field and T is the absolute temperature. Figure 8 shows the variation of drift velocity, electric field and Hall ratio on temperature for electrons and holes. The drift mobility depends on drift velocity and electric field which will change with irradiation, the effect of radiation damage on Lorentz angle is not well understood.

The measurement method for the Lorentz angle measurement is via cluster size measurements. In the absence of a magnetic field, the minimum average cluster size should occur at an incidence angle of zero degrees, i.e. when the track is perpendicular to the wafer surface. When a magnetic field is applied, the Lorentz force will cause the moving charge (both electrons and holes) to deviate by an angle θ_L.
Thus the position of the minimum of the average cluster size will no longer occur at zero degrees of incidence angle, but rather at an incidence angle equal to the Lorentz angle

	Electrons	Holes
$v_s(cm\,s^{-1})$	$1.53 \times 10^9 \times T^{-0.87}$	$1.62 \times 10^8 \times T^{-0.52}$
$E_c(V\,cm^{-1})$	$1.01 \times T^{1.55}$	$1.24 \times T^{1.68}$
β	$2.57 \times 10^{-2} \times T^{0.66}$	$0.46 \times T^{0.17}$
r_H	$1.13 + 0.0008(T - 273)$	$0.72 - 0.0005(T - 273)$

Figure 8: Drift velocity, electric field and Hall ratio on temperature for electrons and holes

θ_L. In order to find the Lorentz angle, the sensor is rotated at different angles to change incidence angle and find the angle corresponding to the minimum cluster size. [Figure 9] shows the Lorentz angle measurement is done on the current ATLAS SCT using cosmics [8].

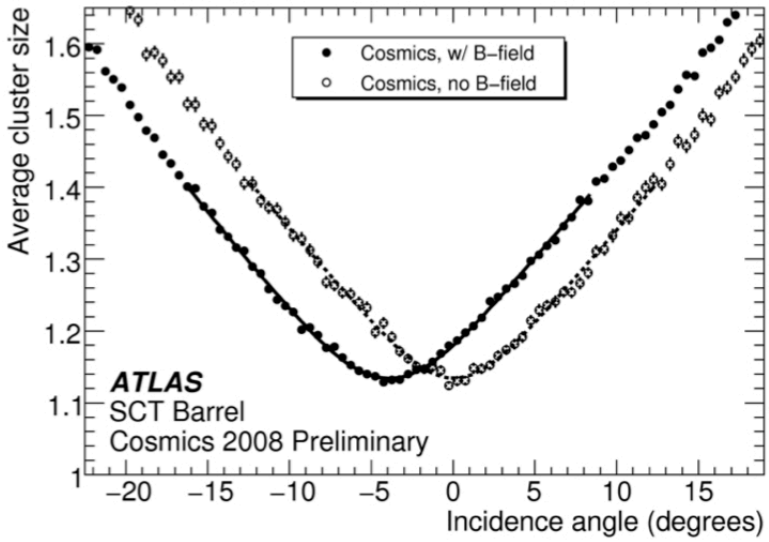

Figure 9: Lorentz angle measurement carried out with the current ATLAS SCT using comics. In the absence of magnetic field we see that the minimum cluster size corresponds to zero angle, however in the presence of magnetic field due to Lorentz force we see that the minimum cluster size corresponds to the Lorentz angle

2.1 Experiment Setup

The Setup consists of the following :

- **Beam**
  Electrons beam from the DESY II test beam facility (1-5 GeV).
- **Magnetic field**
  Magnetic Field from a 1 T superconducting solenoid in test beam area 24/1 .
- **Beam Telescope**
  EUDET beam telescope is used to find the incident angle. The DUT is fixed between telescope planes to the find the angle of incidence as shown in [Figure 11].
- **Device Under Test (DUT)**
  Consists of the following :
  - ATLAS sensor miniature .
  - Alibava Readout System daughter board.
  - Cooling system for irradiated samples. Cooling is important for irradiated samples to prevent annealing and to avoid leakage current.

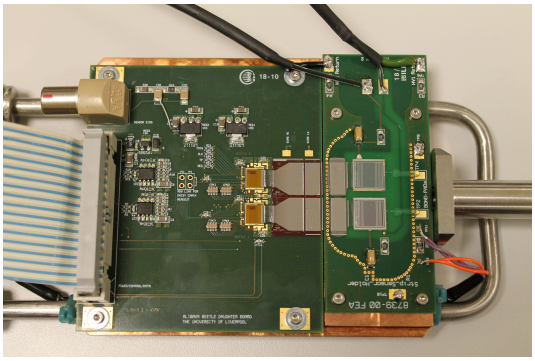

Figure 10: The Alibava daughter board connected to the sensor and cooling pipes

2.2 The Alibava Readout System

The Alibava readout system is an analog readout system used in the Lorentz angle measurement setup. It is a compact and portable readout system . The system can be used with different run types [Figure 12] [9]:

- Radioactive source: external trigger input from one or two photomultipliers. *This is setup used to take data with radioactive source in the laboratory and with beam at the test beam .*

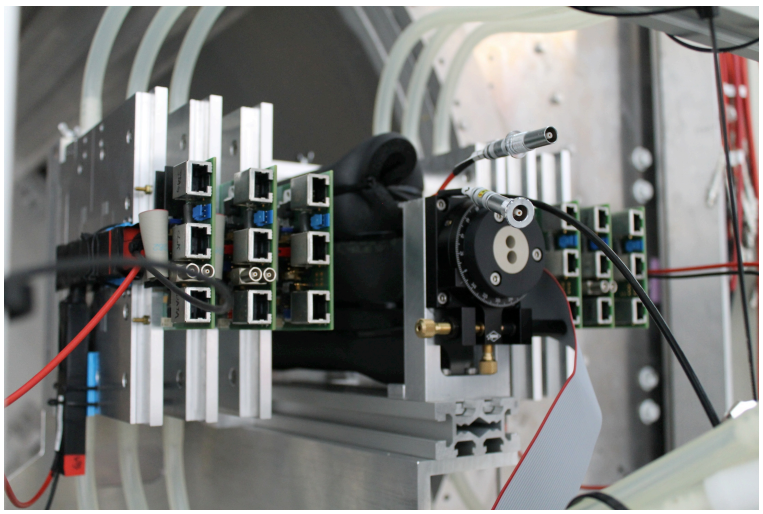

Figure 11: The DUT between telescope planes

.

- Laser system: synchronized trigger output generated internally for pulsing an external excitation source.

The system contains two front-end readout chips (Beetle chip used in LHCb) to acquire the detector signals. It communicates with PC via USB communication which will store and will process the data acquired. The system is controlled from PC via a FPGA that interprets and executes orders. The system has its own power supply system.
The system consists of :
⇒ **Hardware part**

- Daughter board
  A small board that contains two Beetle readout chips (used in LHCb) , has fan-ins and detector support to interface the sensors.
- Mother board
  - Process analogue data that comes from the readout chips
  - Process trigger input signals (RS), generate triggers (Laser).
  - Control hardware part (FPGA) and communicate with PC via USB.

⇒ **Software part** Control the whole system (configuration, calibration amd acquisition). It produces output files for data analysis.

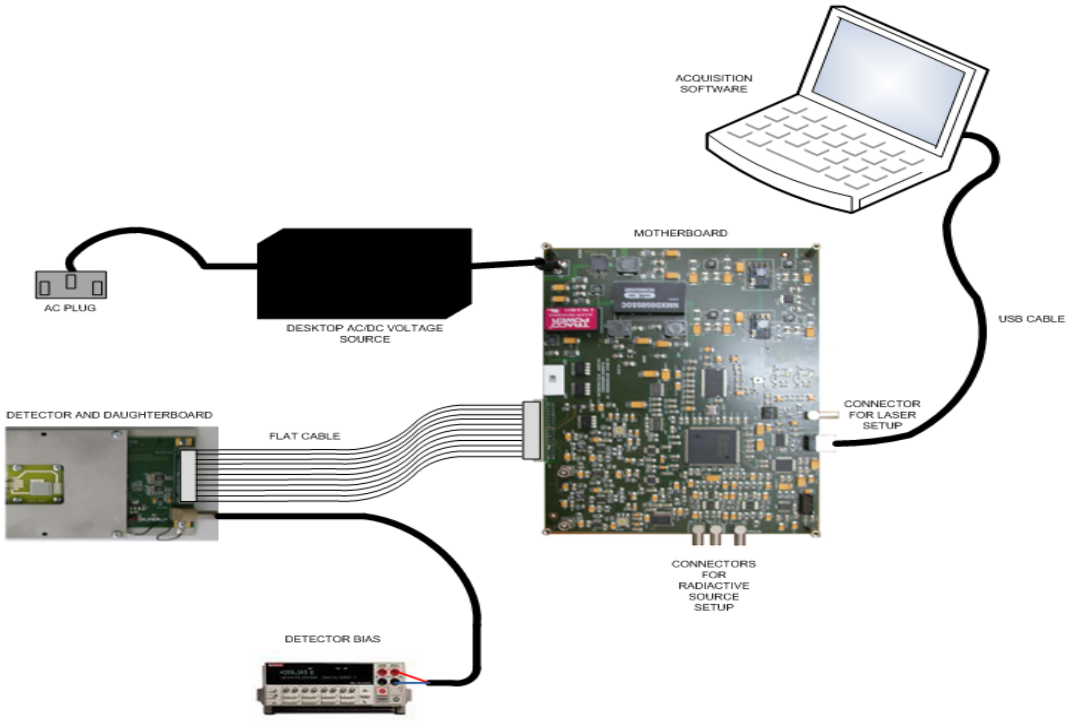

Figure 12: A shcematic overview of the Alibava system components.

.

2.3 Motivation

The Lorentz angle measurement experiment setup is quite complex from data acquisition prospective for a number of reasons :

- Presence of high magnetic field
  The DUT, telescope and cooling pipes will be inside the 1 T solenoid, and because the high magnetic field can affect the Alibava motherboard, it is necessary to separate mother and daughter board with a long cable (11 m) so that the motherboard can be kept in a lower magnetic field area. Therefore, it was very important to investigate the effect of the longer cables on the signal, and to correct the signal in case of changes.

- Cooling
  Part of the setup is to cool the DUT to around -25^oC which is important for irradiated samples to prevent annealing and to avoid leakage current. The presence of such temperatures can affect the signal, so it must be considered to correct for it in case of changes.

3 Calibration of Alibava Readout System

3.1 Method and Procedure

To eliminate the effects of the mentioned setup parameters on the signal, we use calibration method. The aim of calibration is to determine the average signal (in ADCs) per injected charge as shown [Figure 13] which is a screenshot of the calibration run on the Alibava software. This is achieved by a charge injection circuit that injects known amounts of charge and measures the signal for each charge injection [Figure 14] [10].

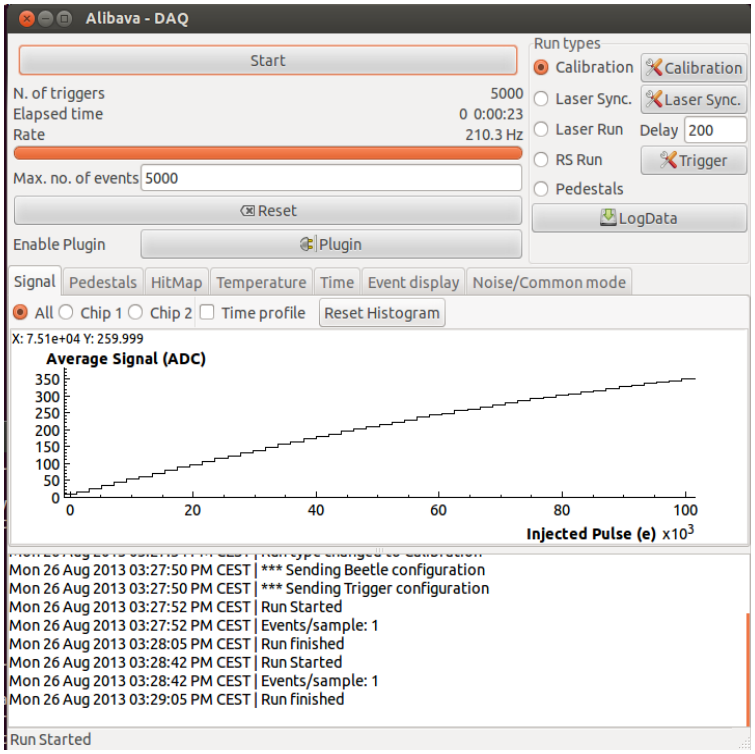

Figure 13: Screenshot of the Alibava software during calibration run.

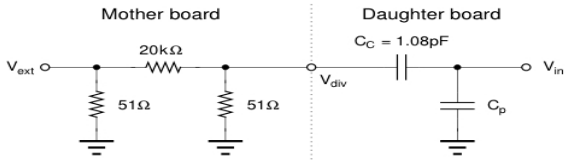

Figure 14: Charge injection circuit.

Charge injection circuit on the test board. The input signal V_{ext} is generated from a digital pattern generator DG2020A [TEK]. V_{in} is connected to the input of the Beetle preamplifier. The terminating resistor as well as the resistive divider is located on the mother board. To minimize the line capacitance of the routing, the coupling and load capacitances are placed very close to the inputs of the Beetle chips on the daughter board.
The detailed schematic of the charge injection input circuit is shown in figure 14. The injected output charge of this circuit is given by

$$Q_{in} = \frac{V_{ext}}{2} \cdot \frac{50}{20000} \cdot C_C \tag{3}$$

where V_{ext} is the output signal of the pattern generator. A voltage step of 2.6 V at V_{ext} and a standard capacitance of 1.08 pF at C_C results in an injected charge Q_{in} of 22345 e^-. This charge corresponds roughly to 1 minimum ionizing particle (MIP), whichh is the standard charge for an external input signal. In accordance to equation (3) the possible charge range of the input circuit is given from 4297e^- to 77351e^-. Other input charges can be generated but require the exchange of the coupling capacitance C_C on the daughter board. Furthermore, the board contains blocking components for power supply lines as well as load capacitance C_p.

3.2 Monitoring of DUT parameters

In order to find out how the signal and calibration values vary with different temperatures, it was necessary to build a monitoring interface using NI LabView . Also, the monitoring is very important to monitor temperature and humidity changes for the cooling process. Monitoring of the humidity of the air inside the DUT is also important to calculate the dew point to prevent condensation of water vapor inside the DUT. To control humidity, a nitrogen source is used to flush the DUT to keep humidity low.
The monitor interface consisted of the following components:

- Sensors (temperature and humidity) mounted inside the DUT.
- NI DAQ system (PXI crate,DMM and switch)
- NI LabView interface [Figure 15].

In addition, a current monitor was needed to monitor the current drawn in each of the telescope planes, therefore current monitor circuit was designed and integrated with the LabView interface software.
Details of the monitoring of DUT parameters on Appendix A.

3.3 Software updates

For data analysis of Alibava data, I used the Alibavasoft package written by Eda Yildirim. The software had to be updated to account for calibration parameters and

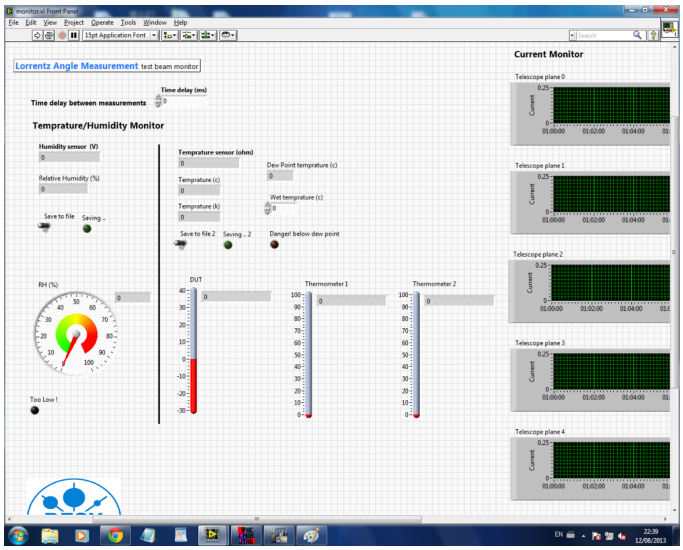

Figure 15: The LabView software interface.

correct the signal accordingly. The software had a number of runs to analyze the data. I used *CalRun* and *PulseShape*. *CalRun* is used to construct calibration data (Charge/ADC) for each channel from calibration file raw data and pedestals file. *PulseShape* is used to reconstruct pulse shape and signal from raw-data file and pedestals file.

For *CalRun*, we first plot charge as a function of ADC for each channel, so we can use the injected charge to correct the change in signal values. Also, in order to make use of the histograms, the charge/ADC histograms are fitted using a linear fit in the range of expected signal (0-200 ADC) which can be changed to other values according to setup. From the linear fit we get a linear equation for charge as function of ADC, and save the slope and offset value of each channel to be used for signal corrections.

For *PulseShape* runs, I implemented calibration corrections in the calculations. Procedure for each channel is to read the calibration constants from calibration run, then to convert ADCs to collected charge.

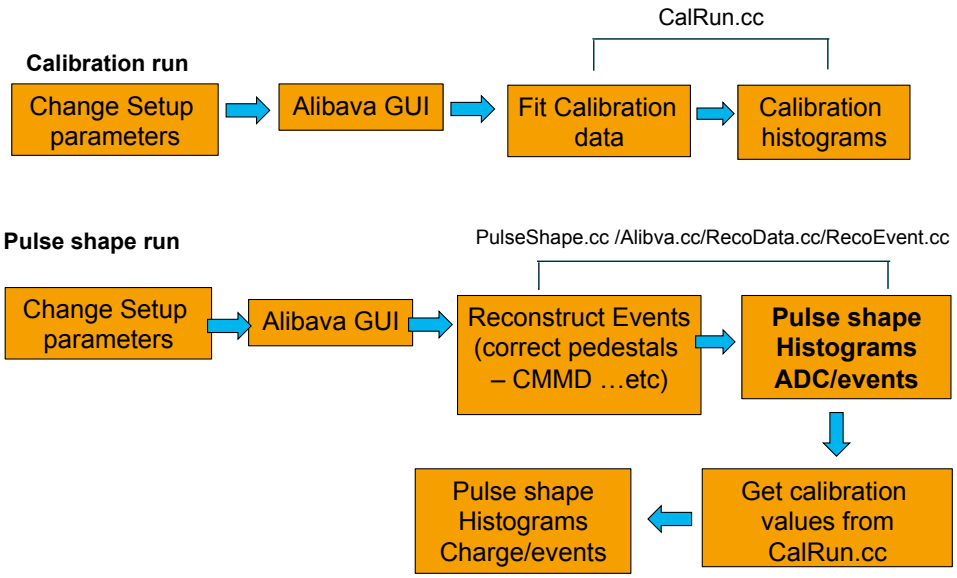

Figure 16: Software update sequence.

.

4 Results

Calibration without cooling The output of the calibration runs is a set of histograms showing the Charge/ADC for each channel. The output histograms after linear fitting is shown in [Figure 17] where we see the relation between injected charge and signal for channel 10. Although, the relation is not linear because of characteristics of readout system, we expect a signal in the region from 0 to 200 ADCs which can be fitted linearly. The linear fit parameters (slope and offset) for each channel is saved in another plot shown in [Figure 18] where slopes of linear fits are shown for all channels. Zero slopes indicate not bonded channels.

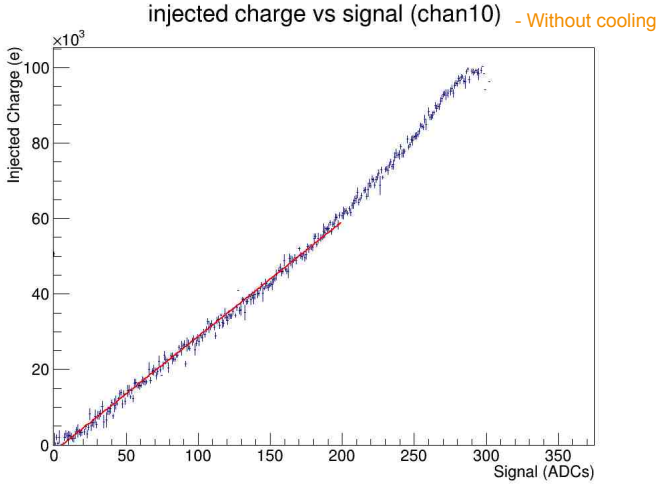

Figure 17: Calibration data for channel 10 with linear fit.

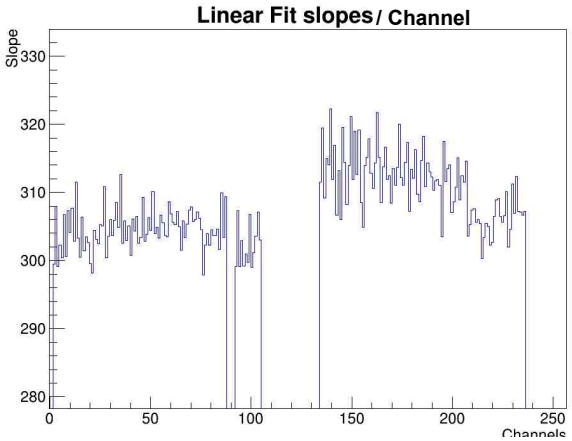

Figure 18: Linear fitting slope for all channels. Zero slopes indicate unbonded channels
.

Cable length dependence To investigate the effect of cable length, I made two calibration runs for a short cable approx. 3 meters long and a long cable approx. 11 meters long which we will need to avoid magnetic field on the Alibava motherboard. Calibration values for channel ten is shown -as above- in [Figure 19] for long and short cable. We see that long cable has a higher slope than short cable, which indicates that for the same amount of injected charge we get more signal in shorter cable. This is because Alibava is an analogue readout system, so signal attenuation in long cable is the reason for this. For all channels linear fit slopes for long and short cables are shown in [Figure 20]

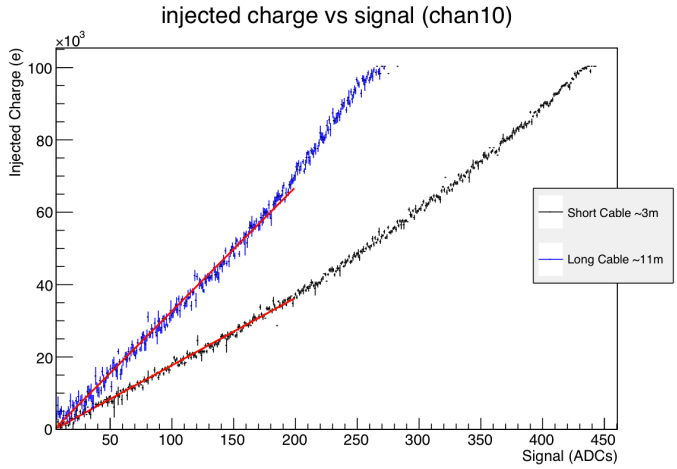

Figure 19: Short cable/Long cable calibration data.

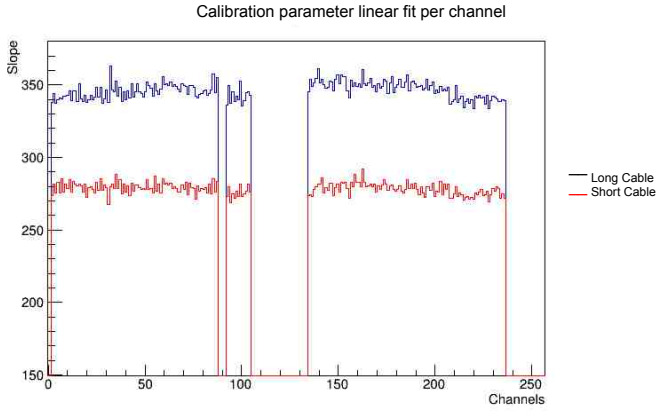

Figure 20: Linear fitting slopes for long and short cable.

The next step was to construct a hit amplitude histogram to compare signals we get from short and long cables before calibration corrections, a hit amplitude is a sum of all events from all channels. We used a radioactive source as a source of electrons Sr-90. The hit amplitudes we got for short and long cables are shown in [Figure 21] where we can see a shift in the value of signal due to signal attenuation in longer cable.

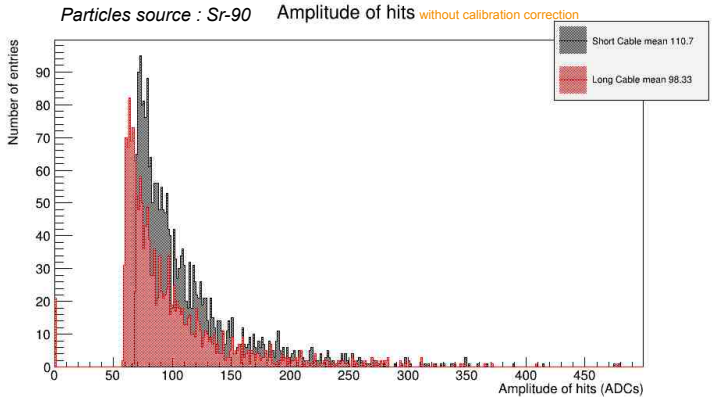

Figure 21: Signal shift between short and long cable.

The signal we get after calibration corrections is shown in [Figure 22], we get the same value of the signal regardless of the cable length, however we loose some events because of the signal to noise ratio.

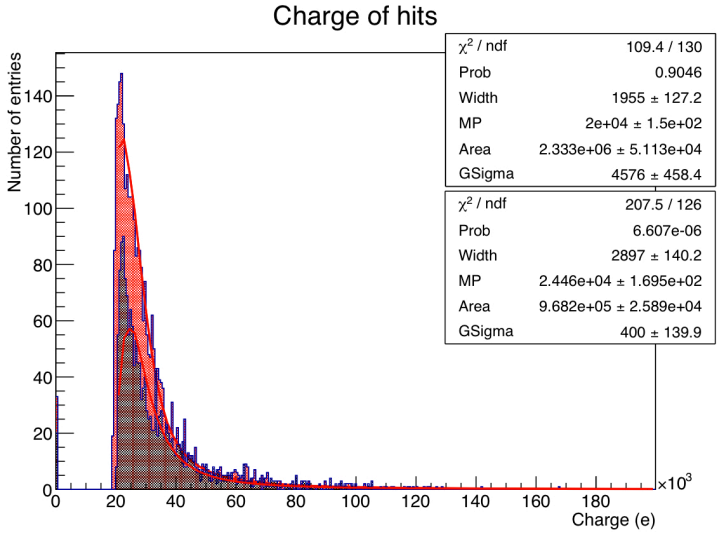

Figure 22: Long and short cable signals after calibration corrections

.

Temperature dependence Same method can be used to correct for temperature effect on signal. Investigating the temperature effect on calibration value we see direct relation between temperature and calibration parameters. In [Figure 23] we see that the slope of calibration data increases with higher temperatures, which indicates that signal increases with lower temperature. For all channels we can linear fit slopes in [Figure 24]. *We had a limited dataset of different temperature because of problems with the chiller used for cooling.*

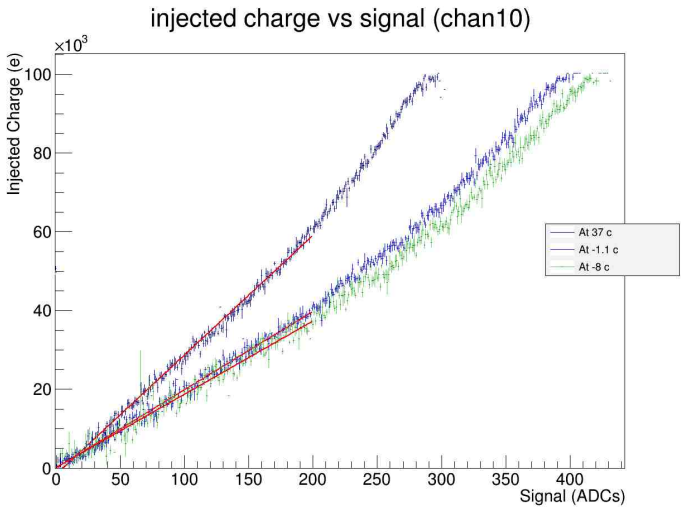

Figure 23: Calibration data at different temperatures

.

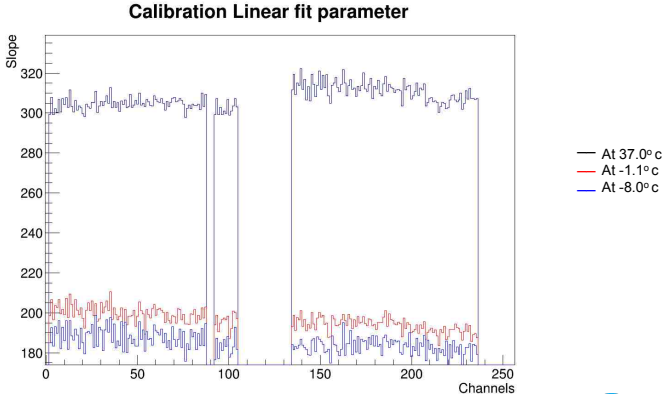

Figure 24: Linear fit slopes at different temperatures

.

Magnetic field dependence For different values of magnetic field the same process was carried out to confirm that magnetic field has no effect on the signal. We had calibration runs without magnetic field and with 0.5 and 1 Tesla. In [Figure 25] we see that calibration data for different magnetic field value are the same. And for all channels we can see that magnetic field does not affect the signal as shown in [Figure 26]

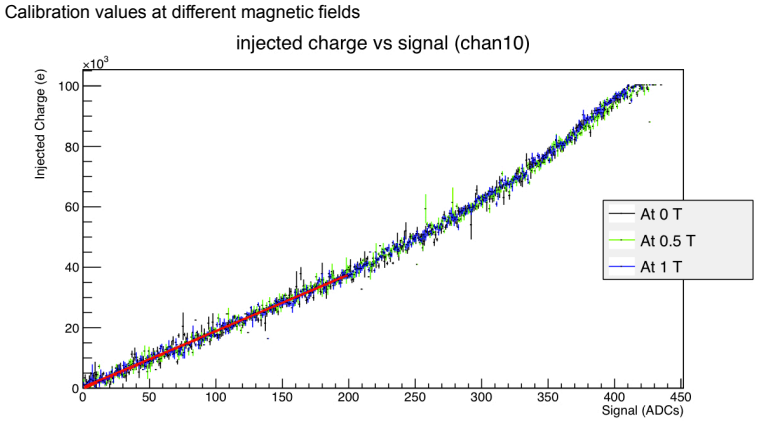

Figure 25: Calibration data at different magnetic fields

.

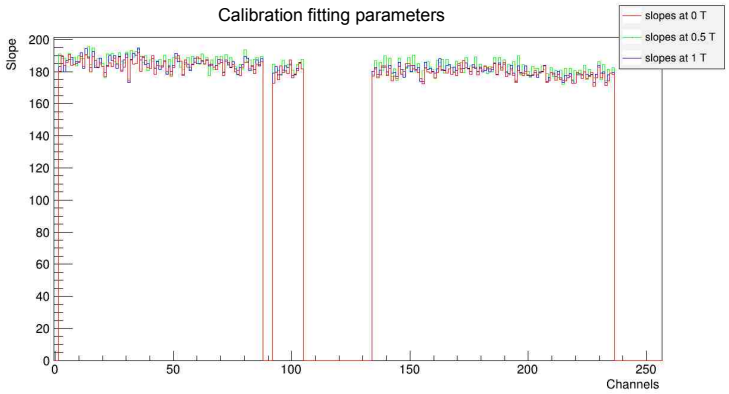

Figure 26: Linear fit slopes at different magnetic field

.

5 Conclusion

The study of Lorentz angle variation under high radiation is important for the accurate reconstruction of particle tracks and momentum for the HL-LHC. Calibration of Alibava readout system is important to account for experiment setup that can affect the signal. Calibration corrections can be applied to correct for signal attenuation in cables. Calibration values differ directly with the temperature of the readout system and cable length. However, it does not change with Magnetic field (as expected). Calibration corrections will be applied in the new version of the analysis software. The LabView VI can be used to monitor temperature on DUT and humidity inside the DUT box to be used with calibration and for monitoring the cooling process. This current monitoring VI can be used with any setup with telescope.

6 Acknowledgments

I would like to thank greatly my supervisor Eda Yildirim for her amazing support and help.
Also, I would like to thank Igor Rubinskiy, Ingrid-maria Gregor and Kerstin Tackmann of the ATLAS team for their great help. I would like to thank Ulrich Koetz for his help. And last but not least Torsten Kuelper for his help in the E-Lab.

7 Appendix: Monitoring of DUT parameters using NI LabView

The NI data acquistion system consists of the following components[Figure 27]:

- **NI PXI create**
  A PC-based platform for measurement and automation system.
- **NI PXI DMM**
  PC-based digital multimeters.
- **NI PXI switch**
  Multiplexers/Relays for multiple readings. The switch can be connected in a number of different topologies (1-wire, 2-wires and 4-wires). The 1-wire topology will give 64 positive leads with a common ground. The 2-wire topology will give 32 pairs of positive and negative leads. 4-wire topology will give 16 channels of 4 leads[Figure 28].

Figure 27: Components of the NI DAQ

.

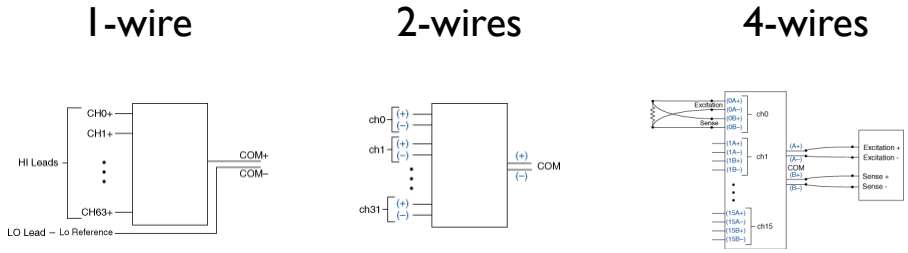

Figure 28: Different topologies of the NI switch

.

The NI LabView software interface used the NI DMM/Switch express VI that uses handshake system for sequenced operation. After every measurement it sends a measurement

finished trigger for the next measurement to start. The virtual instrument consists of the following components as shown in [Figure 29] :

- **NI DMM/Switch express VI** that reads data (i.e. resistance for thermistors or voltage for humidity sensors), the type of measurement can be selected from the DMM tab. From the switch tab at the VI the channel corresponding to the sensor can be selected.
- **NI Formula VI** after the acquisition of sensor raw data, it needs to be converted to a proper value corresponding to sensor type (i.e. resistance to temperature), therefore a formula VI is used where the input is the sensor data, and output the value of the quantity we are measuring.
- **Timed Sequence** for multiple measurements, A DMM/switch VI is added to frames of a timed sequence, the time delay between frames can be specified from the from properties or an empty frame with time delay block can be added.
- **Result Indicators** to display the results we measure from the sensors, we can used the LabView display items (i.e. numeric indicators, gauges ..etc) and connect them to the formula block where the output is the value we are measuring.

For current monitoring of the telescope planes, a current monitoring box was designed using resistors, voltage across each was measured using DMM and conversion to current is done with the resistor values. The current monitor is integrated with the software interface [Figure 30] and can be used to monitor currents for any setup that includes telescope.

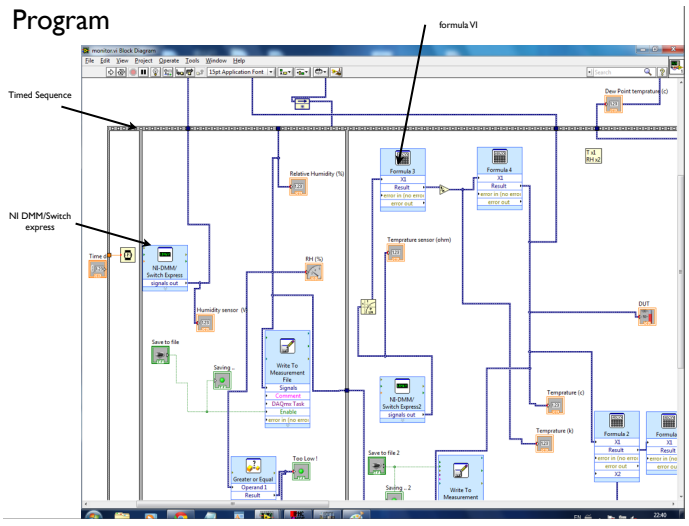

Figure 29: VI Software interface

.

Figure 30: Current monitoring box

.

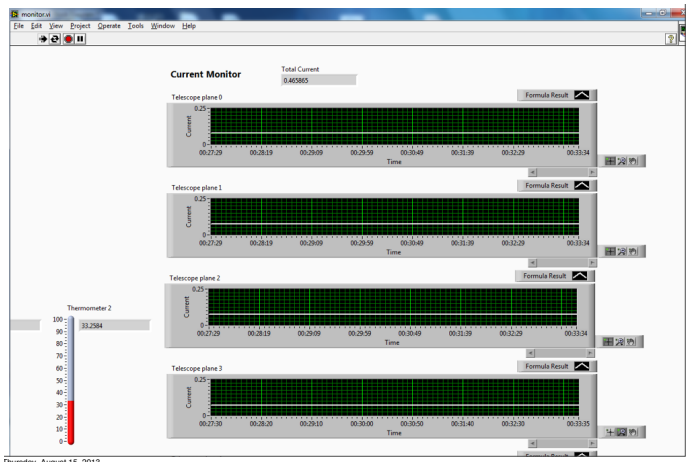

Figure 31: Screenshot of the VI during operation

.

References

[1] Overall detector concept *atlas.web.cern.ch*

[2] ATLAS Inner Detector *atlas.web.cern.ch*

[3] ATLAS Letter of Intent: Phase II Upgrade *CERN-LHCC-2012-022*

[4] ATLAS Letter of Intent: Phase II Upgrade *CERN-LHCC-2012-022*

[5] DPG Dresden March 4,2013 *E.Yildirim*

[6] Lorentz angle variation with electric field for ATLAS silicon detectors *ATL-INDET-2001-004*

[7] ATLAS Letter of Intent: Phase II Upgrade *CERN-LHCC-2012-022*

[8] Lorentz Angle and Cluster Width Studies for the ATLAS SCT *ATL-COM-INDET-2009-039*

[9] Alibava System Hardware 15th RD50 Workshop, 16-19 November 2009, CERN *Marco-Hernndez*

[10] PhD dissertation, University of Heidelberg, Germany *S.L.öchner*